Integrated Geophysical Investigations at the Greek Kamarina Site (Southern Sicily, Italy)

Salvatore Scudero[1] · Raffaele Martorana[1,2] · Patrizia Capizzi[2] · Antonino Pisciotta[3] · Antonino D'Alessandro[1,2] · Carla Bottari[4] · Giovanni Di Stefano[5,6]

[1] Istituto Nazionale di Geofisica e Vulcanologia, Osservatorio Nazionale Terremoti, Via di Vigna Murata 605, 00143 Rome, Italy

[2] Dipartimento di Scienze della Terra e del Mare, Università degli Studi di Palermo, Via Archirafi 20, 90123 Palermo, Italy

[3] Istituto Nazionale di Geofisica e Vulcanologia, Sezione di Palermo, Via Ugo La Malfa 153, 90146 Palermo, Italy

[4] Istituto Nazionale di Geofisica e Vulcanologia, Sezione di Roma 2, Via di Vigna Murata 605, 00143 Rome, Italy

[5] Polo Regionale Museale per i Siti Culturali di Ragusa, Piazza Libertà 2, 97100 Ragusa, Italy

[6] Dipartimento di Studi Umanistici, Università della Calabria, Via P. Bucci, Cubo 28B, 87036 Arcavacata di Rende, Italy

Abstract

Kamarina, located in southern Sicily (Italy), was an important Greek colony since its foundation in the sixth century BC. Archaeological excavations, carried out since the twentieth century, uncovered only limited portions of the site so far. Despite the importance of the Greek colony, the presence of remarkable buildings that archaeologists expected to bring to light has not found fully correspondence in the archaeological excavations. Consequently, the integrated geophysical prospection carried out in the study area is aimed to support and address the future archaeological investigations. After the photographic and thermographic survey obtained by an unmanned aerial vehicle, we performed a systematic survey through ground magnetic and GPR methods over an area of 6200 m^2. The acquisition procedures have been optimized in order to get the best results combining high resolution and elevated speed of acquisition. The results derived from the three geophysical techniques have been conveniently combined by means of a cluster analysis, allowing us to clearly identify a series of buried archaeological features. Because of their geometrical characteristics, often in good agreement with the spatial arrangement of the archaeological remains at the surface, these buried archaeological features can be interpreted as roads, walls, or buildings foundations in which the various construction phases of the city can be clearly recognized. The integrated approach has proven to be essential for a robust interpretation of the archaeogeophysical investigation.

Keywords Archaeogeophysics · Ground magnetic survey · GPR · UAV thermography · Cluster analysis · Kamarina · Sicily

1 Introduction

Since its first applications to archaeology in the 1970s, geophysics provided an essential and valuable support to the archaeological researches, so that today the scientific community commonly refers to those applications as “archaeogeophysics”. The advantages of the geophysical methods to archaeological prospection rely on the non-invasive nature,the rapidity to execution, and the relatively limited cost. An integrated approach, given by the combination of two or more geophysical techniques, allowing us to overcome many of the limitations of each method. Magnetic and ground-penetrating radar (GPR) investiga- tions are the techniques most frequently used in archaeology; they measure, respectively, the contrast of susceptibility between the soil and buried archaeological findings, and the reflection and refraction of electromagnetic pulses due to anthropogenic features. These techniques are based on different principles, are sensitive to different physical properties, and investigate different soil depths. Besides, they are fast and quite effective in the case of a compact, isolated, and depth-limited source: just the kind of source generally occur- ring in archaeological investigations. The obtained information is complementary, and its integration is fundamental to detect all the archaeological features that, otherwise, could be overlooked. The detected anomalies represent a valuable and essential resource in address-ing excavations in archaeological sites not completely studied as the present case study.

In this paper, we report an integrated geophysical investigation focused on the ancient Kamarina settlement (southern Sicily, Italy). Here only limited portions of the whole archaeological site have been investigated so far, and only few civil and public buildings have been brought to light. Since the importance of the site in the Greek age, archaeologists assume the possible presence of imposing structures, but any observable evidence has not supported such a hypothesis so far. The present study is aimed to find evidence of buried archaeological structures and, in particular, to verify the hypothesis of the existence of a Greek theatre probably built in this site, which has been matter of debate among archaeologists. Furthermore, the archaeologists addressed the geophysical prospection in a sector adjacent to the Greek agora (the place where citizens were used to met) since the archaeological evidence suggests that in Kamarina-like Greek cities, the most prominent public edifices were usually grouped together.

The techniques involved are GPR and magnetic survey supported also by the 3D model of the archaeological site and by the thermography relief obtained by means of an unmanned aerial vehicle (UAV). The support of aerial photogrammetry provides an accurate control of the measurements over the surveyed area, a 3D high-resolution reconstruction of the terrain and the outcropping archaeological features (digital surface model, DSM), and the eventual comparison with future archaeological excavations or morphological surveys. The acquired data have been opportunely elaborated in order to isolate and enhance any clue ascribable to archaeological sources.

2 Archaeological and Geological Background

The archaeological site of Kamarina is located onto an almost flat, terraced promontory (named Cammarana hill), gently descending seawards, along the southern coast of Sicily (Italy) (Fig. 1). The promontory (ca. 50 m a.s.l.) extends in a NW–SE direction and is bounded by the Ippari River to the north, the Rifriscolaro River to the south, and the Mediterranean Sea to the west. The geological succession is made up of whitish and grayish marls dated at Middle Miocene, unconformably covered with a layer of terrigenous sand and gravel (Lentini and Carbone 2014); this deposit constitutes the archaeological soil of Kamarina.

According to Thucydides, the Syracusan colonists founded Kamarina at the beginning of the sixth century BC (598–597 BC). The almost complete absence of evidence of an earlier occupation seems to confirm this dating (Pelagatti 1976, 2000). Over the

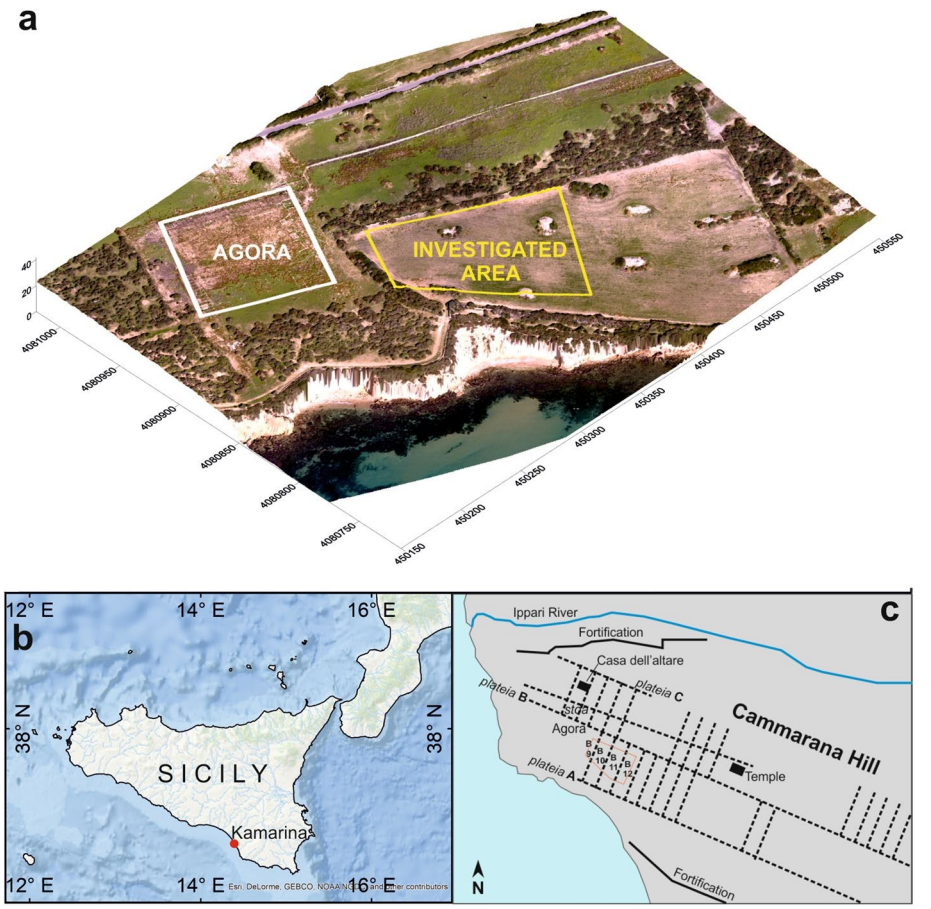

Fig. 1 a 3D view of the orthophoto of the Kamarina archaeological site; **b** location of the site in southern Sicily; **c** planimetry of the ancient urban pattern in the north-western termination of the Cammarana hill (from Pisani et al. 2008)

fifth century BC, Kamarina progressively gained significance and prestige as testified by the commercial exchanges, indeed its strategic location in southern Sicily allowed to control the traffic on the Mediterranean Sea for many centuries. The city reached its maximum urban expansion at the end of the fourth century BC, during the Hellenistic period. The Romans conquered the city in 258 BC and rebuilt the city after its partial destruction. But Kamarina gradually lost its importance, and in the Augustan period, the city, now greatly reduced in size, was finally abandoned together with the entire coastal area of south-eastern Sicily (Di Stefano 1994). However, the channel-harbour, constructed in the Greek age by adapting the mouth of the Ippari River, survived and

became the hub for important commercial traffics during the Roman age, remaining in use for a longer time. Kamarina was definitively destroyed after the Arabic conquest of Sicily in 827 AD. Afterwards, the site has been deeply exploited as a quarry for construction material during the Middle Age and up to the fifteenth and sixteenth century.

The archaeological interest in the ancient Kamarina started in the sixteenth century and increased in the following century, when the first documented archaeological excavations were carried out at the site and it became an attractive destination for many travellers. During the late eighteenth and the nineteenth centuries, numerous excavations took place in various parts of the ancient city, but the systematic excavation of the town began only later thanks to Paolo Orsi in 1896 (Cordano 2013). At present, only limited portions of the whole archaeological site have been investigated. Among them, the ruins of the Temple of Athena located on top of the Cammarana hill (c.f. Pelegatti 1985); the agora placed at the south-western end of the hill between the Athena temple and the harbour; the southern portion of the city fortification walls at the southern foot of the hill (Di Stefano 2000, 2006). The archaeological site became regional interest in the early 1970s; today a museum hosts a rich collection of the archaeological finds retrieved at the site (Pelagatti et al. 2006). Recently, the part of the promontory facing the sea has undergone to a rapid coastal erosion caused by the construction of a new harbour along the shoreline, which has altered the natural coastal circulation system. Nowadays a part of the archaeological area is threatening to slide into the sea, urging archaeologists and institutions to take timely actions and proper measures to protect the archaeological heritage of the ancient Kamarina and ensure its preservation for the present and future generations.

3 Geophysical Surveys

The present multi-technique geophysical study is aimed at integrating the capabilities of the various methods, overcoming their single limitations in highlighting the buried archaeological features such as depth of investigation, spatial resolution, or contrast between the buried archaeological features and the hosting terrain (Sala et al. 2012; Garrison 2016). The archaeogeophysical studies increasingly include an integrated approach rather than a single-technique investigation (Sambuelli et al. 1999; Chianese et al. 2004; Rizzo et al. 2005; Capizzi et al. 2007; Nuzzo et al. 2009; Capizzi et al. 2012; Capizzi and Martorana 2014; Ekinci et al. 2014; Piga et al. 2014; Cella and Fedi 2015; Leucci et al. 2015; Ranieri et al. 2016; Khouas et al. 2017; Vermeulen et al. 2017; Welc et al. 2017; Bottari et al. 2018). In almost all the papers including an integrated approach, the GPR survey represents the most employed technique, followed by the magnetic method; other techniques are usually less used and sometime provide only a secondary support. However, all the data obtained from the different geophysical methods can be combined with statistical correlative approach allowing a more comprehensive and robust interpretation of the geophysical results, being the anomalies better outlined and constrained.

In the Kamarina archaeological site, we first performed the aerial photographic survey in order to build a detailed digital surface model (DSM) and to properly position the geophysical investigations, namely the aerial thermographic survey, the GPR, and the magnetic survey.

The survey area extends for about 6200 m^2 on the southern slope of the Cammarana hill, between the sacred urban area and the public open space of the *agora* where no other modern archaeological investigations were carried out before (Fig. 1). In particular, the investigations were performed just south of one of the recognized main Greek road axis (called

plateia B). According to the reconstruction of the urban network (Fig. 1c), in this area we should expect to intersect three orthogonal secondary roads (*stenopoi* B9–10, B10–11, and B11–12) and the neighbourhoods (insula) in between. The ground is constituted by a sandy matrix with heterogeneous pebbles and abundant earthenware fragments. At the present time, the area is cultivated and the soil is periodically ploughed. The geophysical surveys were carried out during three different campaigns in a time span of about 4 months: from June to November 2017. In the following paragraphs, we give the details of the application of each geophysical investigation, describing the acquisition, the processing, the results, and finally, presenting the interpretation.

3.1 Aerial Photographic and Thermographic Survey

The recent development in the use of unmanned aerial vehicles (UAVs) for remote sensing applications provides new opportunities for mapping and monitoring because of the rapidity of survey, the reduced costs, and the ultra-high resolution (Nex and Remondino 2014). Among the possible applications with UAVs, photogrammetry is a very effective tool in archaeological prospection (c.f. Fernández-Hernandez et al. 2015; Campana 2017). The aerial photographic and thermographic surveys of Kamarina were performed in order to produce a high-resolution digital surface model (DSM) of the archaeological site. The thermography is a less frequently used method in archaeogeophysics; however, in some conditions, the aerial thermal images can reveal a wide range of both surface and shallow subsurface, archaeological features and other cultural landscape elements. The thermal mapping performed from UAV platforms is a really recent development, allowing us to survey over a much larger area in much less time (Poirier et al. 2013; Casana et al. 2017; Thomas 2017). Such a favourable combination allows the use of thermal prospection for archaeological detection at low altitude with high-resolution information, from a microregional scale to a single site scale. The high potential is regarding the detection of archaeological structures whose presence is manifested on the surface by differences in temperature. In detail, the application of thermography to archaeology is based on the differences in rate of absorption, emission, transmission, and reflection of thermal infrared radiation of the archaeological features with respect to the surrounding terrain. Such differences depend ultimately on the composition, density, and moisture content, of the materials on, and below, the ground surface. The fluctuations of the thermal infrared radiation depend on several external variables, and it is not always easy to isolate the archaeological source within the thermal signal. However, if adequately processed, the anomalies associated with archaeological features can be somehow enhanced (Casana et al. 2014; Cool 2015).

The survey system consists in a lightweight UAV (1.1 kg) equipped with an on-board digital camera, GPS, and autopilot system. The UAV is a quadcopter Phantom 3 Dji, well suited for photogrammetry and mapping (Lens FOV 94°—20 mm, Sony Sensor EXMOR 1/2.3", effective pixel resolution of 12.4 Mpx). The data acquisition was accomplished by a combination of two missions in a uniform crossed grid pattern. The coverage of the entire area has been achieved by the acquisition of 5400 frames. The location of a set of artificial control targets was determined using a GPS NAVCOM SF-3040 with angular accuracy of 1 cm, and their positions were used to geo-reference the digital model. The flights have been performed at an altitude of 30 m and at a speed of 3 m/s. Photograph overlap is user set in the 75–85% range, allowing the high-quality photogrammetric image matching. The aerial photographs were processed into georeferenced orthoimages, a high-resolution DSM and digital elevation model (DEM), using the photogrammetric 3D reconstruction technology software by AgiSoft PhotoScan (Agisoft 2013). The DSM generated has a ground resolution up to 4.0 cm (Fig. 1). Advances in computer vision and image analysis are,

however, generating innovative developments in photogrammetry through the technique of structure from motion (SfM), which offers an automated method for the production of high-resolution digital surface models (DSMs) with standard cameras (Fonstad et al. 2013; Javernick et al. 2014; Micheletti et al. 2015). The DSM was extended not only over the investigated portion of the site, but across the whole archaeological area (Fig. 1).

The aerial thermal survey has been performed with the same UAV, equipped with a thermal imaging camera Optris PI 640 with an optical resolution of 640 × 480 pixels. The PI 640 delivers pin-sharp radiometric pictures and videos in real time with frame rate up to 32 Hz. The spectral range is 7.5–13 μm, the temperature range from − 20 to 1500 °C, with accuracy of ± 2 °C. The flight was executed at speed of 2.5 m/s and 30 m of elevation. Images can easily become blurred if the camera moves too quickly during the flight and, at the same time, the automated alignment of thermal images in photogrammetric software is facilitated (overlap of 70–80% between adjacent images).

The thermal radiation from the Sun is absorbed and then emitted from the ground soil, depending on the thermal properties of the involved materials. On the bare soil, the ground surface temperature can be assumed as a result of the analytical application of the physical laws of the thermal exchange (Périsset and Tabbagh 1981; Bellerby et al. 1990); conversely, the vegetation acts as a filter concealing the useful information coming from ground surface and subsurface (Cool 2015). The study area is almost completely bare; however, we have been performing several surveys under different situations in order to get the optimal environmental conditions. We finally process and show the results of a thermographic survey (a whole of 120 frames) taken during a morning flight when the superficial effects due to diurnal flux variations are minimized, but the temperatures of the various materials are still adjusting so that their differences are emphasized (Tabbagh 1977). The aerial thermal survey flight lasts approximately 60 min, during which we can assume that the environmental conditions were constant. Theoretically, the maximum depth for a detectable anomaly at surface is function primarily of the thickness and thermal diffusivity of the soil and of the buried features, of the magnitude and rate of the heat flux, while it marginally depends on the frequency of the radiation (Bellerby et al. 1990). The soil thermal diffusivity is controlled by several factors (e.g., composition, density, and moisture content) and usually is in the order of 10^{-7} m^2 s^{-1} but can vary by a factor of 20 (Sorour et al. 1990), so that the depth at which subsurface archaeological features can be resolved varies considerably. Experimental data suggest that, under favourable conditions, the diurnal heat flux will reach at least the upper 50 cm of the soil profile (Périsset and Tabbagh 1981; Bellerby et al. 1990). At the same time, longer-term transient heat flux over a period of several days may reveal features at considerably greater depth: even though not directly resenting from the external radiation, features may be detected since they affects the proprieties of the shallower layer (Scollar et al. 1990).

3.2 Magnetic Survey

Magnetometry is one of the most widely employed geophysical techniques in archaeology (c.f. Godio and Piro 2005; Kvamme 2006; Gaffney 2008; Fedi et al. 2017 for a complete review). The technique is able to detect buried anthropic structures through the analysis of the anomalies in the Earth's magnetic field because anthropogenic features have usually different magnetic properties from the cover terrain. For this research, the magnetic survey was carried out by means of the Overhauser magnetometer–gradiometer GEM-19 from GEM Systems which has an accuracy of 0.2 nT. The Overhauser effect magnetometer exploits the effect of the proton precession. By adding free electrons (free radicals) to

the measurement fluid, the nuclear Overhauser effect can be used to significantly improve the performance with respect to the proton precession magnetometer. The sensors are two cylindrical coils and contain a proton-rich liquid solvent which is combined with free radicals to increase the signal intensity. A low-power radio-frequency field is used to polarize the electron spin of the free radicals, which then couples to the protons via the Overhauser effect. The main advantages of this type of magnetometer are the accuracy of measurements, the fast sampling rate, and the minimum power consumption that, in turn, allows lightweight batteries for portable device. For all these reasons, this device is particularly suitable for applications in archaeogeophysics (Smekalova et al. 2008).

The device was set as gradiometer with two parallel sensors spaced by 56 cm and carried by the operator on a specific backpack. The same operator performed the two surveys (June and October 2017) to ensure the same height of the sensors from the ground. The sensors are oriented orthogonally to the progress direction, so that they have the same arrangement in the roundtrip tracks. Measurements were taken walking along parallel lines spaced by 0.5 m and materialized on the field with measuring tapes. The magnetometer is equipped with a GPS providing the position and the time for each magnetic measure (5 Hz sampling frequency). At this frequency, and considering the walking pace of the operator, the measures are located on average at every ~ 16 cm along the progress direction. The overall setting of the magnetic survey, that is the sampling frequency, the distance between the two sensors, and the profile spacing, has been chosen in order to bring out the magnetic features at very shallow depth.

The survey resulted in 240 magnetic profiles and more than 86,000 readings. A shift of about − 20nT was affecting the October 2017 measurements with respect to the June 2017 ones. Temporal magnetic variations due to perturbations in the ionosphere and magnetosphere affect the magnetic observations (Campbell 2003; Love 2008); such variations are commonly referred as “diurnal variations” although the period is variable. In order to homogenize the results, the measurements were then corrected compensating the differences in the observed values in the overlapping area.

The magnetic profiles are affected by noise. Many of the noise sources are essentially point sources such localized high magnetic minerals in the surface soils or ferrous objects (Hinze et al. 2013), and this is very probable in an archaeological soil. Therefore, the outliers were removed with an automated despiking and each profile filtered with a moving average (Fig. 2, top). The bidirectional acquiring mode (i.e.roundtrip walking) caused a typical noise due to the different symmetry, along adjacent lines, of the instrument–operator system. This generates maps showing a typical “striping” (“heading error”; Scollar et al. 1990). Such amplitude shift is ascribable to the non-perfect parallelism of the sensors between the two opposite directions of progress, partly due to the undulating paths and partly to the pitching of the sensors while walking. Therefore, the adjacent profiles were corrected, in pairs, by equalizing at the same mean value the data acquired along each line of the measured field (Ciminale and Loddo 2001). Another error, typical of the bidirectional mode, was probably due to a systematic error in the positioning of the measurements, caused by an offset between the position of GPS system and the sensors. This generated a typical “zigzag effect” that was corrected by using a statistical method based on cross-correlation (Ciminale and Loddo 2001). Figure 2, bottom, shows an example of correction for the bidirectional mode. The whole set of 240 profiles is then interpolated with a polynomial regression to draw a rough map of the total magnetic field and of the vertical magnetic gradient. A stripe of anomalous low magnetic values in the southernmost part of the study area is clearly referable to the presence of a metal fencing delimiting the archaeological site, and therefore, anomalous data have been removed in the following elaboration.

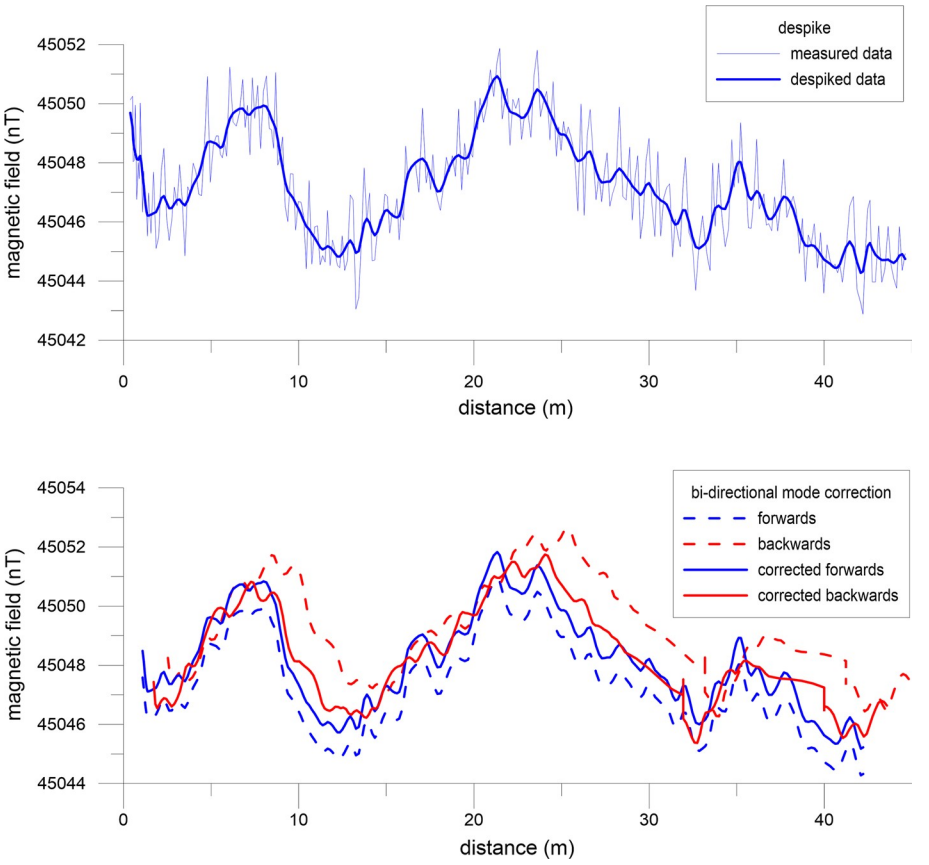

Fig. 2 Top: example of smoothing of a magnetic profile with a moving average; bottom: example of the bidirectional mode corrections in two adjacent magnetic profiles carried out in opposite directions

3.3 Ground-Penetrating Radar survey

Ground-penetrating radar technology (GPR) is probably the most common technique in archaeogeophysics for its ability to solve the subsurface structure with good resolution, reconstruct 3D models, and, also because it can be easily applied in a wide range of situations (Capizzi et al. 2012; Dojack 2012; Conyers 2013; Garrison 2016; Ranieri et al. 2016). GPR is able to detect discontinuities in the magnetic impedance of the subsurface through the propagation and reflection of electromagnetic waves. A transmitter generates the waves; then, the amplitudes and the time delays of the reflected waves at objects and interfaces are recorded.

For this research, the GPR survey was performed using a SIR-3000 system from GSSI, equipped with a 400 MHz antenna. The antenna has been selected according to the resolutions and depth of investigation. The entire survey area was then georeferenced on the DSM by means of high-precision portable GPS measurements. The direction of the GPR profiles is parallel to the direction of the magnetic profiles. In the first campaign, the profiles were carried out along traces 0.5 m spaced, according to hypothetical average size

of the buried archaeological structures. After the comparison between the results with the 0.5-m profile spacing with a wider spacing (1.0 m) over a test area, we have been able to assess that the capability to detect buried structures is unaltered and the loss of resolution is acceptable. Therefore, by doubling the spacing we halved the survey time.

The acquired data were processed with background removal and band-pass filters. Then, the 2D profiles have been rearranged in time slices (Goodman et al. 1995) to obtain a three-dimensional model of the electromagnetic reflectivity of the shallow subsoil, until a depth of about 2 m. By analysing the main reflection hyperbola, we considered an average velocity of 0.07 m/ns for the electromagnetic waves to convert the time slices into depth slices.

4 Geophysical Results

The geophysical prospection allowed us to identify several anomalies ascribable to buried archaeological features. In this paragraph, we present the results and compare the characteristics (size, geometry, and depth) of the buried archaeological structures highlighted by the different techniques.

The acquired magnetic data have been corrected and interpolated to draw a map of the total magnetic field. But for their successful interpretation is fundamental a processing that could isolate and enhance the anomalies (Ciminale and Loddo 2001). The reduction to the magnetic pole (RTP), first proposed by Baranov (1957), is a widely used filter able to transform the observations as if they were obtained at the geomagnetic pole, where the vector of the magnetic field is perpendicular to the Earth's surface. In fact, owing to the inclination and declination of the Earth's magnetic field, the magnetic anomalies relative to a source have reduced amplitude, are bipolar or asymmetric, and are shifted to the south in the northern geomagnetic hemisphere. Therefore, after the RTP correction the anomalies are centred over their sources. The values of the RTP map range from about 45,030 to 45,065 nT (Fig. 3). The map shows a general, large-scale negative gradient moving southwards probably ascribable to a large-scale geological source. There is evidence of medium-size (in the order of 10^1 m) and small-size magnetic features (in the order of 10^0 m) with magnitude of few nT up to ~15 nT. In particular, small-scale, linear, magnetic features are recognizable in proximity of the northern and eastern corners of the study area. They are mainly arranged along the ~NE–SW direction and secondary along the ~NW–SE orthogonal direction. Furthermore, larger anomalies are present in the central part of the investigated area: an arc-shaped negative anomaly with convexity to the NE and a circular positive anomaly more to the east. We show also the map of the magnetic gradient (Fig. 4) where many of the magnetic features detected in the RTP map (Fig. 3) are also recognizable, although less evident because the acquired gradiometric data are affected by a relatively high noise. Similarly to the RTP, we calculated the 3D analytical signal of the total magnetic field (Nabighian 1984; Roest et al. 1992), which does not require any assumption with regard to the magnetization. The analytic signal is calculated combining the magnetic gradient in the three directions; the amplitude is given by the square root of the sum of the squares of the three derivatives. The amplitude (or energy envelope) of the analytic signal is independent from the phase anomaly, and its maximum is located on the vertical of the source of the anomalous signal. Actually what we calculated is a pseudo-analytical signal since the magnetometer provides only the total value of the magnetic field rather than its three components; therefore, the three gradients were not measured, but calculated. The map of the analytical signal is not clear as we expected just because of the high noise level

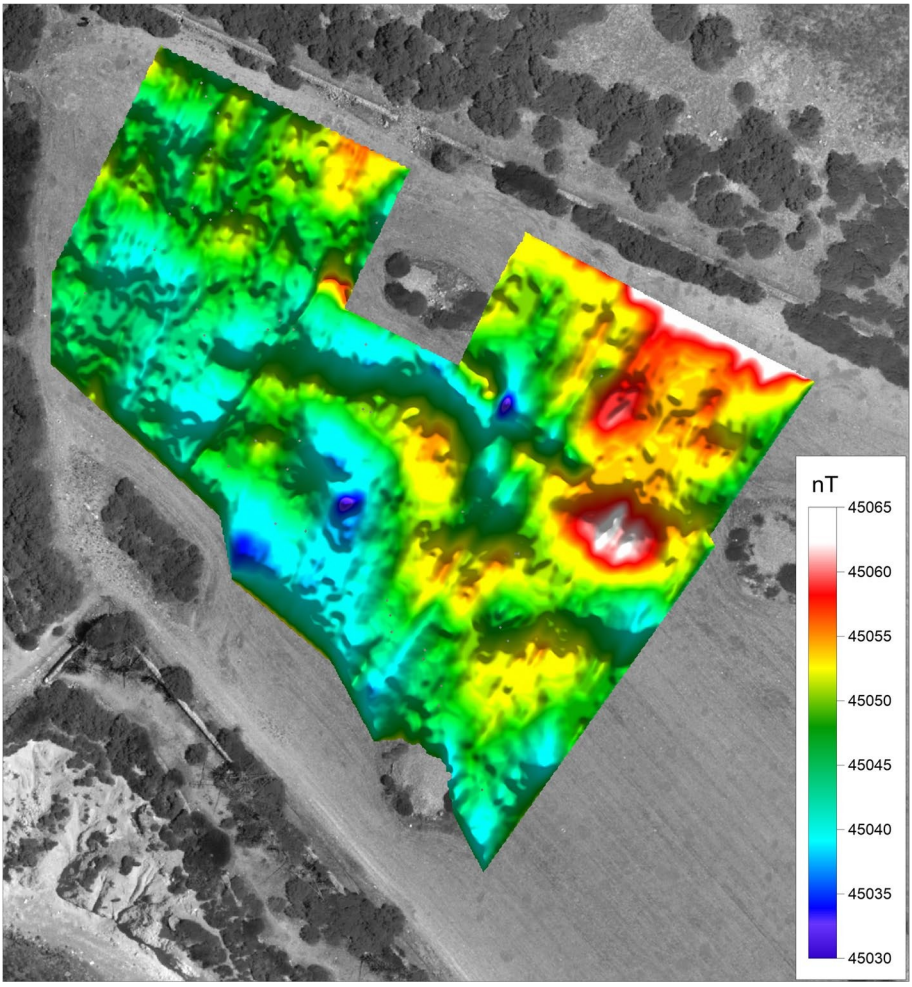

Fig. 3 Reduction to the magnetic pole (RTP) map

of the vertical gradient data. Consequently, we calculated the horizontal gradient map by combining exclusively the two horizontal derivatives (Fig. 5). This latter map is the one that better highlights the magnetic anomalies due to near surface structures. The two sets of linear features (~ NE–SW and NE–SW) form some quadrangular boxes located along the north-eastern boundary. Also the arc-shaped and the circular anomalies already evidenced in Fig. 3 are well outlined.

The shallowest time slices of the GPR model show significant anomalies for interpretation purposes. In particular, we considered three time slices: a shallower at 6–12 ns, an intermediate at 12–18 ns, and a deeper at 18–24 ns. Considering a velocity of about 0.07 m/ns, these correspond to depth slices at about 20–40, 40–60, and 60–80 cm, respectively. In the shallower slice (Fig. 6a) are clearly recognizable some reflectivity responses along straight alignments, sometime with orthogonal arrangement forming box-shaped elements; these are mainly located in the northern and north-eastern parts of the study area.

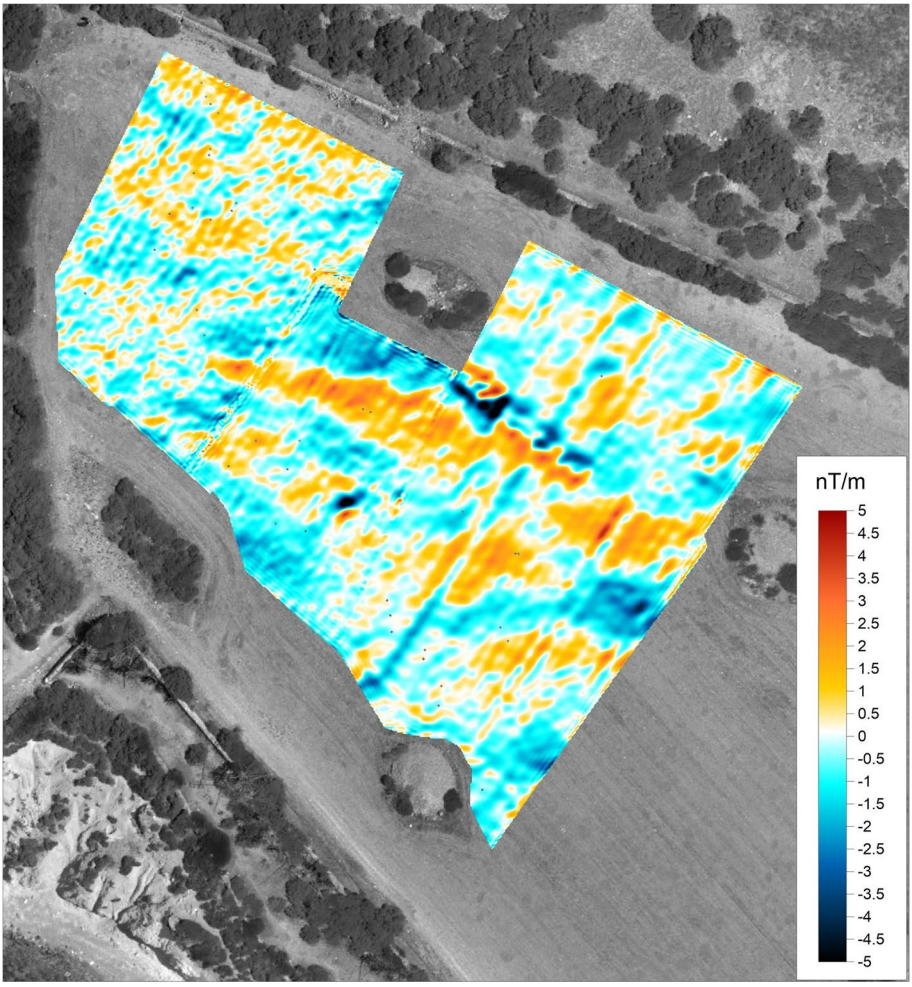

Fig. 4 Magnetic gradient map

These features appear even more significantly in the intermediate slice (Fig. 6b), where is recognizable also the arc-shaped anomaly, 6–8 m wide, observed also in the magnetic data. The shallower anomalies disappear in the deeper slice (Fig. 6c), whereas the larger arc-shaped anomaly is still persistent. Figure 6d summarizes the three slices in a 3D volume rendering.

Finally, the thermal infrared map (Fig. 7) shows how the temperature is primarily influenced by the land coverage. However, we can exclude any possible effects due to the vegetation in the investigated area, essentially characterized by the bare land. The ground temperature ranges from 16 to 20 °C, while the linear NW–SE pattern is due to the ploughing. Some thermal features are recognizable on the map, ranging on the order of 1–3 °C. The interpretation of thermal maps is not always straightforward: the amplitude and the sign of a given thermal anomaly depend on the contrast between the thermal inertias of the buried feature and of the cover layer. The amplitude of the anomaly increases with the contrast, and it is positive

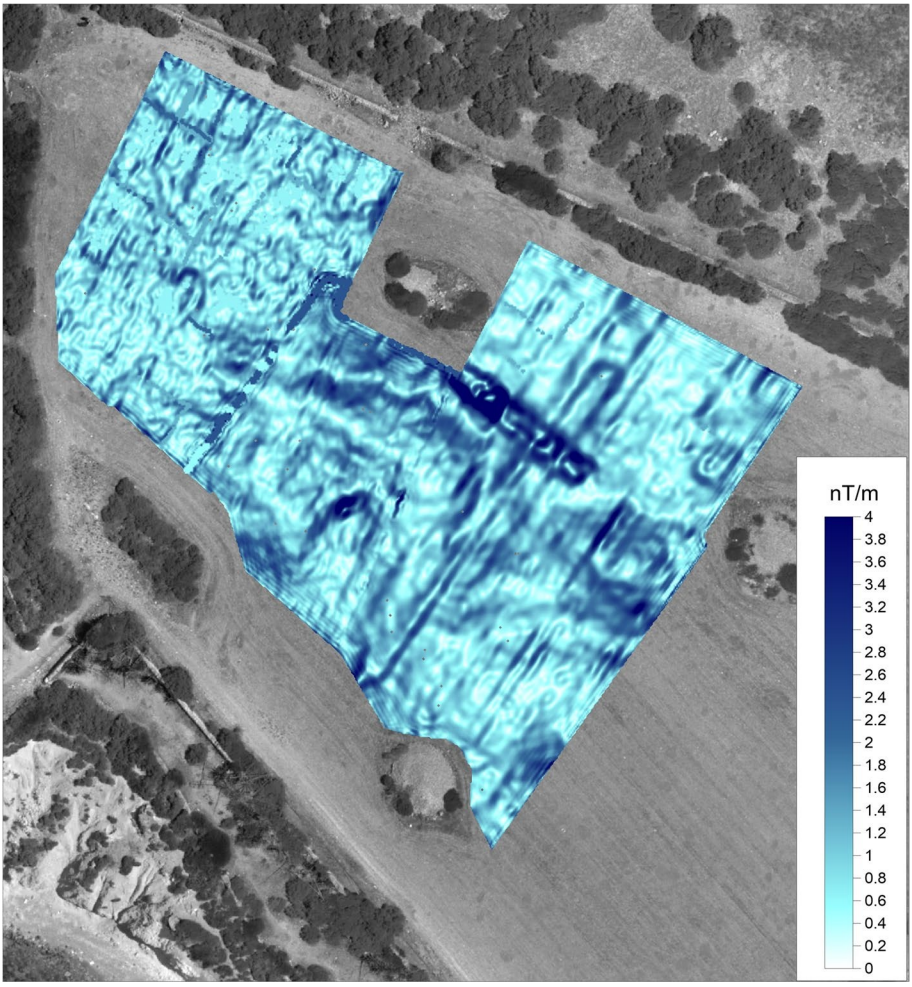

Fig. 5 Horizontal gradient map

when the soil is gaining heat (positive flux); conversely, the anomaly is negative when the soil is losing heat (Périsset and Tabbagh 1981). Not knowing the values of the proprieties of the involved materials, it is not possible to directly interpret the thermal map in Fig. 7. Therefore, we combined the results of the thermal survey together with the results coming from the other methods so that the identification of the archaeological features is better constrained and the following archaeological interpretation would be more robust.

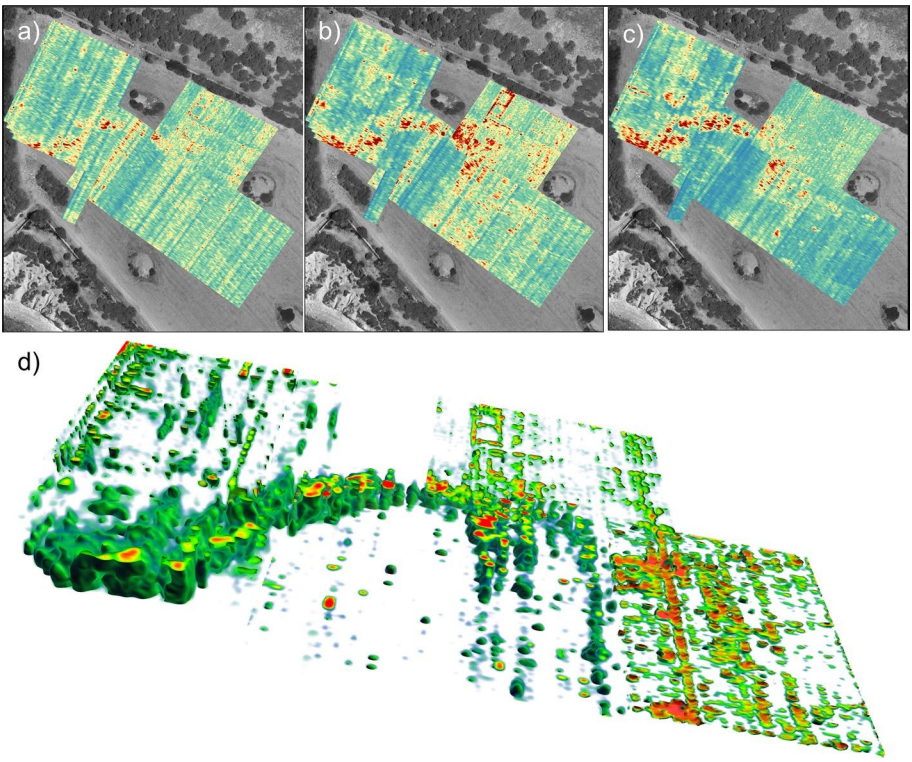

Fig. 6 **a** GPR depth slice ranging from 20 to 40 cm depth; **b** GPR depth slice ranging from 40 to 60 cm depth; **c** GPR depth slice ranging from 60 to 80 cm depth; **d** 3D view of a GPR isosurface

5 Cluster Analysis

The results obtained with the various methods have been integrated by means of a centroid-based clustering approach in order to obtain more robust constraints on the highlighted anomalies. The procedure of clustering allows the identification, within a set of objects, of some subsets called clusters, that tend to be homogeneous among them, exhibiting a high internal (i.e. intra-cluster) consistency and high external (i.e. inter-cluster) heterogeneity (Barbarito 1999). Generally, the cluster analysis does not require an a priori interpretative model (Fabbris 1983). The centroid-based clustering technique can be formally regarded as an optimization problem: (1) find the k cluster centres and associate each object to its cluster, such that the squared distances from the cluster centroid are minimized; (2) calculate the new averages to be the centroids of the observations in the new clusters. The algorithm reaches a (local) optimum when the assignments no longer change; however, there is no guarantee to find the global optimum.

A modified centroid-based algorithm has been applied to the magnetic, GPR, and thermal data. Concerning the magnetic data, we selected the horizontal gradient map (Fig. 5) because it is less noisy with respect to the vertical one and the magnetic anomalies are clearer. For GPR, the maxima values among the three slices shown in Fig. 6 are considered.

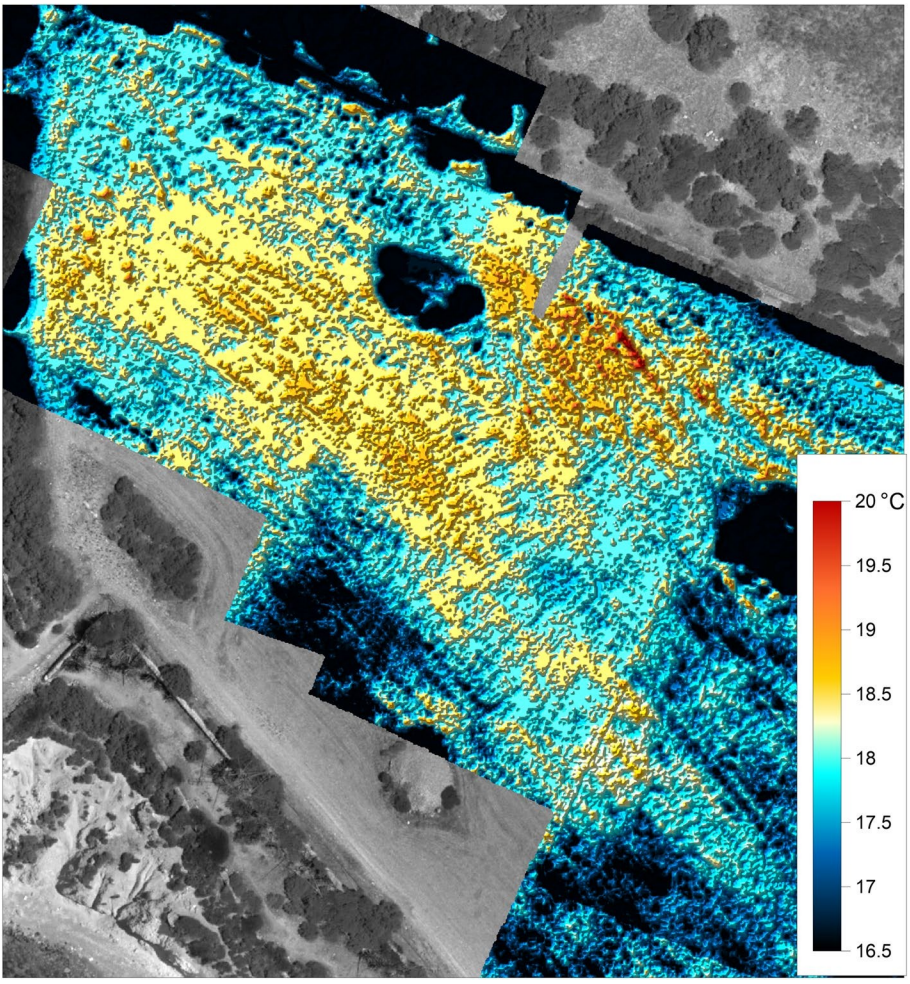

Fig. 7 Thermal infrared map

The distance of each element from the initial nuclei and the nuclei obtained after each iteration was calculated by the weighted sum of the Euclidean distances of all considered parameters:

$$D = a\ dx^2 + dy^2\ ^{1/2} + b\ dM^2\ ^{1/2} + c\ dR^2\ ^{1/2} + d\ dT^2\ ^{1/2}$$

where a, b, c, and d are the weights, dx, dy, dM, dR, and dT are the differences between the spatial coordinates (x and y), the horizontal magnetic gradient, the electromagnetic reflectivity, and the ground surface temperature, respectively.

The biggest drawback of centroid-based algorithms is the choice of the number of clusters (k) and the initial centroid coordinates. Therefore, it is important to run diagnostic checks for determining the appropriate number of clusters in the data set. The proposed algorithm does not fix the number of k clusters and choose automatically for each k the

Fig. 8 **a** Result of the cluster analysis ($k=7$) correlating the three survey methods; **b** sketch of the detected features: the red lines indicate the features inferred after the cluster analysis; the purple lines indicate the features highlighted by GPR survey but not clearly depicted by the cluster analysis; continuous and dashed lines refer to more evident and less evident features, respectively. The black dashed lines indicate the road (stenopos) pattern in the Greek city

initial centroids from the data set (Capizzi et al. 2014, 2017). The shape, size, and number of the clusters, as well the occurrence of outliers, the level of overlap between clusters, and the type of measure of similarity/distance chosen, are all factors that could to affect the results of cluster analysis.

Since the resolution of both the horizontal magnetic gradient and of the GPR is not uniform across the study area, their assigned weights have been differentiated: the magnetic gradient's weight is higher in the western part, whereas the GPR's weight is higher in the eastern sector. Moreover, the values of the horizontal magnetic gradient have been normalized according to a logarithmic scale in order to account also for the small-scale features shown in Fig. 6.

Cluster analysis has been applied only in the areas investigated by all three survey methods (magnetometry, GPR, and thermography). Although it is not possible to determine the best solution in statistical terms, the weights for the distance calculation have been iteratively adjusted so as to obtain the best visualization of the buried archaeological structures (Fig. 8). Cluster analysis made it possible to correlate structures identified by the different survey techniques used, substantially improving the archaeological interpretation.

For completeness, in Fig. 8b some structures identified by the GPR investigations have been reported, in areas not investigated by magnetometry.

6 Archaeological Interpretation

The correlation between magnetic, electromagnetic, and thermal data shows a general agreement of the detected features, even though the results are not always coherent. Figure 8 combines the horizontal magnetic gradient, the maxima values among the three GPR slices, and the thermography: the box-shaped pattern with a NW–SE and a NE–SW arrangement is consistent in the north-western and eastern part of the area, and also the arc-shaped structure is clearly visible in the cluster analysis (Fig. 8b). Figure 8b summarizes the detected features: the red lines indicate the identified elements after the cluster analysis, while the purple lines highlight the features detected by GPR survey but not clearly depicted, or even falling outside, by the cluster analysis. The continuous and dashed lines refer to features more evident and less evident, respectively. For most of the identified features, the reflective bodies highlighted by the GPR survey are also the sources of the magnetic anomalies.

Because of their geometry and size, the small-scale linear anomalies are undoubtedly ascribable to shallow-buried archaeological structures such as roads, walls, or building foundations. The overlap of the identified anomalies with the ancient urban pattern (Fig. 8b), the neighbourhoods of the classic and post-classic period (i.e. the third and the fourth building phase of the city of Kamarina), suggests several interesting hypotheses.

The NE–SW linear elements likely outline the road network of the second and third construction phases spanning from 416 BC to fourth–third century BC (Di Stefano 2006). The other sets of linear element, oriented about NW–SE, are mainly evidenced by the GPR method (c.f. Fig. 6); then, they are shallower and more recent. They could be referable

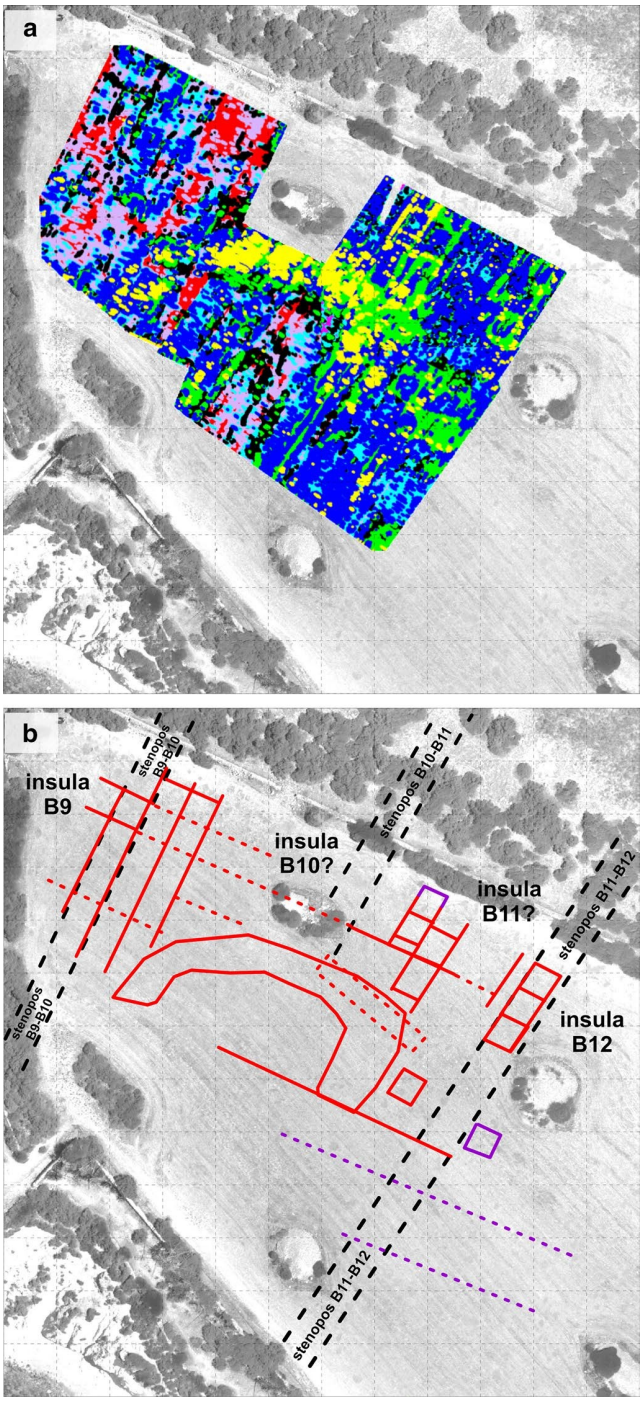
a
b
insula
B9
insula
B10?
insula
B11?
insula
B12
stenopos
B9-B10
stenopos B10-B11
stenopos B11-B12
stenopos
B9-B10
stenopos B11-B12

to the last (i.e. the fourth) construction phase of the city, after the Roman conquest and the consequent partial destruction of the city dated at 258 BC. This phase, ending during the Augustan period, is well documented in the history of Kamarina (c.f. Di Stefano 2006), especially along the *plateia* B and north of the *agora*. This last phase implicates a realignment around the *plateia* B, in the portion between the temple and the *agora*, few degrees counterclockwise with respect to the previous phases (Pelagatti 1976; Di Stefano 2006). For instance, the Greek *stoa*, a covered walkway located in the northern sector of the *agora*, was partly dissected by the opening of a new roman road after this realignment, while the rest of the *agora* was still in use (Di Stefano 2006). Therefore, in such a reconstruction would be identified the eastern limit of the *insula* B9, part of the *stenopos* B9–10, the two entire *insula* B10 and B11, until the *stenopos* B11–12 (Fig. 1c). The elements within the various *insula* represent the single houses of the neighbourhoods, confirming the hypothesis of the urban expansion, after the classical period, over the whole Cammarana hill (Pelagatti et al. 2006).

The arc-shaped anomaly visible in the central portion of the investigated area (Fig. 8) is located within the *insulae* B10 and B11. Its dimensions are about 50 m by 15 m along the maximum and minimum axis, respectively, and it could be consistent with a deeper, larger scale, architectural element. However, no hypotheses on such a structure can be put forward even though we cannot exclude the occurrence of a large public edifice dated to the classical Greek period (before 258 BC).

7 Concluding Remarks

The main goal of this study was to investigate the archaeological site of Kamarina through a multi-technique geophysical survey in order to detect buried archaeological features and verify the existence of structures and, if ever, of the remains, a Greek theatre, whose presence has been matter of debate among archaeologists and scholars. The integration between the magnetic and electromagnetic methods proves to be an effective and reliable tool in the detection of shallow-buried archaeological structures. Conversely, the thermal infrared method, although is fast and easy tool for archaeological investigation, probably does not provide the same capability to reveal buried archaeological structures.

Summarizing, the geophysical prospection of the Greek Kamarina site and the statistical approach for results analysis revealed the presence of numerous buried archaeological structures, well fitting with the four construction phases of the city proposed by the archaeologists. In particular, the outlines of at least three roads and two neighbourhoods are clearly detected, as well as an unidentified larger structure in the central part of the survey area. However, only the direct excavation in situ, exactly addressed by this study, could give the absolute confirmation of our archaeological interpretation.

Acknowledgements We thank Roberto D'Anna (Istituto Nazionale di Geofisica e Vulcanologia, Centro Nazionale Terremoti, Roma) for his help during fieldworks. We also thank Rita Deiana for the editorial handling of the manuscript and two anonymous reviewers for their helpful comments.

References

Agisoft (2013) Agisoft website <http://www.agisoft.ru>. St. Petersburg, 2015

Baranov V (1957) A new method for interpretation of aeromagnetic maps: pseudo-gravimetric anomalies. Geophysics 22(2):359–382

Barbarito L (1999) L'analisi di Settore: Metodologia E Applicazioni. Franco Angeli, Milano

Bellerby TJ, Noel M, Branigan K (1990) A thermal method for archaeological prospection: preliminary investigations. Archaeometry 32(2):191–203

Bottari C, Albano M, Capizzi P, D'Alessandro A, Doumaz F, Martorana R, Moro M, Saroli M (2018) Recognition of earthquake-induced damage in the Abakainon necropolis (NE Sicily): results from geomorphological, geophysical and numerical analyses. Pure appl Geophys 175:133–148. https://doi.org/10.1007/s00024-017-1653-4

Campana S (2017) Drones in archaeology. State-of-the-art and future perspectives. Archaeol Prospect 24:275–296. https://doi.org/10.1002/arp.1569

Campbell WH (2003) Introduction to geomagnetic fields. Cambridge University Press, Cambridge. ISBN: 0-521-82206-8

Capizzi P, Martorana R (2014) Integration of constrained electrical and seismic tomographies to study the landslide affecting the Cathedral of Agrigento. J Geophys Eng 11:045009. https://doi.org/10.1088/1742-2132/11/4/045009

Capizzi P, Cosentino PL, Fiandaca G, Martorana R, Messina P, Vassallo S (2007) Geophysical investigations at the Himera archaeological site, northern Sicily. Near Surf Geophys 5(6):417–426. ISSN 1569–4445. https://doi.org/10.3997/1873-0604.2007024

Capizzi P, Martorana R, Messina P, Cosentino PL (2012) Geophysical and geotechnical investigations to support the restoration project of the Roman "Villa del Casale", Piazza Armerina, Sicily, Italy. Near Surf Geophys 10(2):145–160. ISSN: 1569–4445. https://doi.org/10.3997/1873-0604.2011038

Capizzi P, Martorana R, Stassi G, D'Alessandro A. Luzio D (2014) Centroid-based cluster analysis of HVSR data for seismic microzonation. In: Near surface geoscience 2014—20th European meeting of environmental and engineering geophysics, pp 351–355. https://doi.org/10.3997/2214-4609.201413734

Capizzi P, Martorana R, Carollo A, Vattano M (2017) Cluster analysis for cavity detection using seismic refraction and electrical resistivity tomography. In: 23rd European meeting of environmental and engineering geophysics 2017. https://doi.org/10.3997/2214-4609.201702123

Casana J, Kantner J, Wiewel A, Cothren J (2014) Archaeological aerial thermography: a case study at the Chaco-era Blue J community, New Mexico. J Archaeol Sci 45:207–219

Casana J, Wiewel A, Cool A, Hill AC, Fisher KD, Laugier EJ (2017) Archaeological aerial thermography in theory and practice. Adv Archaeol Pract 5(4):310–327

Cella F, Fedi M (2015) High-resolution geophysical 3D imaging for archaeology by magnetic and EM data: the case of the iron age settlement of Torre Galli, Southern Italy. Surv Geophys 36(6):831–850

Chianese D, D'Emilio MG, Di Salvia S, Lapenna V, Ragosta M, Rizzo E (2004) Magnetic mapping, Ground Penetrating Radar surveys and magnetic susceptibility measurements for the study of the archaeological site of Serra di Vaglio (Southern Italy). J Archaeol Sci 31(5):633–643

Ciminale MA, Loddo M (2001) Aspects of magnetic data processing. Archaeol Prospect 8(4):239–246

Conyers LB (2013) Ground-penetrating radar for archaeology. Wiley, Hoboken. https://doi.org/10.1002/9781118949993

Cool AC (2015) Aerial thermography in archaeological prospection: applications & processing, Doctoral dissertation, University of Arkansas, p 1157. http://scholarworks.uark.edu/etd/1157. Accessed 22 May 2018

Cordano F (2013) Kamarina. In: Bagnall RS, Brodersen K, Champion CB, Erskine A, Huebner SR (eds) The encyclopedia of ancient history. Blackwell Publishing Ltd, Hoboken, pp 3686–3687. https://doi.org/10.1002/9781444338386.wbeah04159

Di Stefano G (1994) Distribuzione e tipologia degli insediamenti di età repubblicana ed imperiale sull'altopiano Ibleo. Publications de l'École française de Rome 196(1):237–242

Di Stefano G (2000) I recenti scavi di Camarina. In: Un ponte fra l'Italia e la Grecia. Atti del Simposio in onore d i Antonino Di Vita, Ragusa 13–15 Febbraio 1999, Padova, pp 195–212

Di Stefano G (2006) Aspetti urbanistici e topografici per la storia di Camarina. In: Pelagatti P, Di Stefano G, De Lachenal L (eds) Camarina 2600 anni dopo la fondazione, Nuovi studi sulla città e sul territorio. Atti del convegno internazionale (Ragusa 7 Dicembre 2002—1–9 Aprile 2003), Roma, pp 157–176

Dojack L (2012) Ground penetrating radar theory, data collection, processing, and interpretation: a guide for archaeologists. Doctoral dissertation, University of British Columbia. https://doi.org/10.14288/1.0086065

Ekinci YL, Balkaya Ç, Şeren A, Kaya MA, Lightfoot CS (2014) Geomagnetic and geoelectrical prospection for buried archaeological remains on the Upper City of Amorium, a Byzantine city in midwestern Turkey. J Geophys Eng 11(1):015012

Fabbris L (1983) Analisi Esplorativa di Dati Multidimensionali. Cleup, Padova

Fedi M, Cella F, Florio G, Manna ML, Paoletti V (2017) Geomagnetometry for archaeology. In: Masini N, Soldovieri F (eds) Sensing the past, vol 16. Geotechnologies and the environment. Springer, Cham

Fernández-Hernandez J, González-Aguilera D, Rodrìguez-Gonzálvez P, Mancera-Taboada J (2015) Image-based modelling from unmanned aerial vehicle (UAV) photogrammetry: an effective. Low-cost tool for archaeological applications. Archaeometry 57(1):128–145

Fonstad MA, Dietrich JT, Courville BC, Jensen JL, Carbonneau PE (2013) Topographic structure from motion: a new development in photogrammetric measurement. Earth Surf Process Landforms 38:421–430

Gaffney C (2008) Detecting trends in the prediction of the buried past: a review of geophysical techniques in archaeology. Archaeometry 50(2):313–336

Garrison E (2016) Techniques in archaeological geology. In: Wagner GA, Miller CE, Schutkowski H (eds) Natural science in archaeology. Springer, Berlin Heidelberg, pp 115–143. ISSN: 1613-9712. https://doi.org/10.1007/978-3-319-30232-4_5

Godio A, Piro S (2005) Integrated data processing for archeological magnetic surveys. Lead Edge 24(11):1138–1144

Goodman D, Nishimura Y, Rogers JO (1995) GPR time-slices in archaeological prospection. Archaeol Prospect 2:85–89

Hinze WJ, Von Frese RR, Saad AH (2013) Gravity and magnetic exploration: principles, practices, and applications. Cambridge University Press, Cambridge. ISBN: 978-0-521-87101-3

Javernick L, Brasington J, Caruso B (2014) Modeling the topography of shallow braided rivers using structure-from-motion photogrammetry. Geomorphology 213:166–182

Khouas A, Hamoudi M, Khaldaoui F, Mihoubi H, Hadji YR (2017) Subsurface geophysics applied to archaeological investigation of Thabudeos Roman fortress (Biskra, Algeria). Arab J Geosci 10(23):522. https://doi.org/10.1007/s12517-017-3260-1

Kvamme KL (2006) Magnetometry: nature's gift to archaeology. In: Johnson J (ed) Remote sensing in archaeology: an explicitly North American perspective. University of Alabama Press, Tuscaloosa, pp 205–223

Lentini F, Carbone S (2014) Geologia della Sicilia-Geology of Sicily. Memorie Descr Carta Geologica d'Italia 95:7–414

Leucci G, Masini N, Rizzo E, Capozzoli L, De Martino G, De Giorgi L, Marzo C, Roubis D, Sogliani F (2015) Integrated archaeogeophysical approach for the study of a medieval monastic settlement in Basilicata. Open Archaeol 1(1):236–246. https://doi.org/10.1515/opar-2015-0014

Love JJ (2008) Magnetic monitoring of Earth and space. Phys Today 61(2):31

Micheletti N, Chandler JH, Lane SN (2015) Structure from motion (SfM) photogrammetry. In: Clarke LE, Nield JM (eds) Geomorphological techniques, Chap. 2, Sec. 2.2. British Society for Geomorphology, London. ISSN: 2047-0371

Nabighian MN (1984) Toward a three-dimensional automatic interpretation of potential field data via generalized Hilbert transforms: fundamental relations. Geophysics 49(6):780–786

Nex F, Remondino F (2014) UAV for 3D mapping applications: a review. Appl Geomat 6(1):1–15. https://doi.org/10.1007/s12518-013-0120-x

Nuzzo L, Leucci G, Negri S (2009) GPR, ERT and magnetic investigations inside the Martyrium of St Philip, Hierapolis, Turkey. Archaeol Prospect 16(3):177–192

Pelagatti P (1976) Sul parco archeologico di Camarina. Le fasi edilizie dell'abitato greco. BA 61:124–126

Pelagatti P (1985) Ricerche nel quartiere orientale di Naxos e nell'agorà di Camarina. Kokalos 30–31(2):679–680

Pelagatti P (2000) Camarina nel VI e V secolo. Problemi di cronologia alla luce della documentazione archeologica. In: Un ponte fra l'Italia e la Grecia. Atti del Simposio in onored i Antonino Di Vita, Ragusa 13–15 Febbraio 1999, Padova, pp 173–190

Pelagatti P, Di Stefano G, De Lachenal L (2006) Camarina 2600 anni dopo la fondazione. Nuovi studi sulla città e sul territorio. Edited by Istituto Poligrafico e Zecca dello Stato, Italy, ISBN: 9788824010207

Périsset MC, Tabbagh A (1981) Interpretation of thermal prospection on bare soils. Archaeometry 23(2):169–187

Piga C, Piroddi L, Pompianu E, Ranieri G, Stocco S, Trogu A (2014) Integrated geophysical and aerial sensing methods for archaeology: a case history in the Punic Site of Villamar (Sardinia, Italy). Remote Sens 6(11):10986–11012

Pisani M, Pelagatti P, Di Stefano G (2008) Camarina: le terrecotte figurate e la ceramica da una fornace di V e IV secolo aC, vol 164. L'Erma di Bretschneider, Rome
Poirier N, Hautefeuille F, Calastrenc C (2013) Low altitude thermal survey by means of an automated unmanned aerial vehicle for the detection of archaeological buried structures. Archaeol Prospect 20(4):303–307
Ranieri G, Godio A, Loddo F, Stocco S, Casas A, Capizzi P, Messina P, Orfila M, Cau MA, Chávez ME (2016) Geophysical prospection of the Roman city of Pollentia, Alcúdia (Mallorca, Balearic Islands, Spain). J Appl Geophys 134:125–135
Rizzo E, Chianese D, Lapenna V (2005) Magnetic, GPR and geoelectrical measurements for studying the archaeological site of 'Masseria Nigro' (Viggiano, Southern Italy). Near Surf Geophys 3(1):13–19
Roest WR, Verhoef J, Pilkington M (1992) Magnetic interpretation using the 3-D analytic signal. Geophysics 57(1):116–125
Sala R, Garcia E, Tamba R (2012) Archaeological geophysics-from basics to new perspectives. In: Ollich-Castanyer I (ed) Archaeology, new approaches in theory and techniques. InTech, Rijeka. ISBN: 978-953-51-0590-9. https://doi.org/10.5772/2412
Sambuelli L, Socco LV, Brecciaroli L (1999) Acquisition and processing of electric, magnetic and GPR data on a Roman site (Victimulae, Salussola, Biella). J Appl Geophys 41:189–204
Scollar I, Tabbagh A, Hesse A, Herzog I (1990) Archaeological prospecting and remote sensing. Cambridge University Press, Cambridge
Smekalova TN, Voss O, Smekalov SL (2008) Magnetic surveying in archaeology: more than 10 years of using the Overhauser GSM-19 gradiometer. Wormianum, Aarhus. ISBN: 978-87-89531-29-8
Sorour MM, Saleh MM, Mahmoud RA (1990) Thermal conductivity and diffusivity of soil. Int Commun Heat Mass Transf 17(2):189–199
Tabbagh A (1977) Sur la détermination du moment de mesure favorable et l'interprétation des résultats en prospection thermique archéologique. Annales de Géophysique 33:243–254
Thomas H (2017) Some like it hot: the impact of next generation FLIR systems thermal cameras on archaeological thermography. Archaeol Prospect 2017:1–7. https://doi.org/10.1002/arp.1588
Vermeulen F, Pincé P, Weekers L, Dapper M (2017) Geoarchaeological study of abandoned Roman urban and suburban contexts from central Adriatic Italy. Geoarchaeology 33:85–99. https://doi.org/10.1002/gea.21642
Welc F, Mieszkowski R, Vrkljan GL, Konestra A (2017) An attempt to integration of different geophysical methods (magnetic, GPR and ERT); a case study from the late Roman settlement on the Island of Rab in Croatia. Studia Quaternaria 34(1):47–59

Terms and Conditions

Springer Nature journal content, brought to you courtesy of Springer Nature Customer Service Center GmbH (“Springer Nature”).

Springer Nature supports a reasonable amount of sharing of research papers by authors, subscribers and authorised users (“Users”), for small-scale personal, non-commercial use provided that all copyright, trade and service marks and other proprietary notices are maintained. By accessing, sharing, receiving or otherwise using the Springer Nature journal content you agree to these terms of use (“Terms”). For these purposes, Springer Nature considers academic use (by researchers and students) to be non-commercial.

These Terms are supplementary and will apply in addition to any applicable website terms and conditions, a relevant site licence or a personal subscription. These Terms will prevail over any conflict or ambiguity with regards to the relevant terms, a site licence or a personal subscription (to the extent of the conflict or ambiguity only). For Creative Commons-licensed articles, the terms of the Creative Commons license used will apply.

We collect and use personal data to provide access to the Springer Nature journal content. We may also use these personal data internally within ResearchGate and Springer Nature and as agreed share it, in an anonymised way, for purposes of tracking, analysis and reporting. We will not otherwise disclose your personal data outside the ResearchGate or the Springer Nature group of companies unless we have your permission as detailed in the Privacy Policy.

While Users may use the Springer Nature journal content for small scale, personal non-commercial use, it is important to note that Users may not:

1. use such content for the purpose of providing other users with access on a regular or large scale basis or as a means to circumvent access control;
2. use such content where to do so would be considered a criminal or statutory offence in any jurisdiction, or gives rise to civil liability, or is otherwise unlawful;
3. falsely or misleadingly imply or suggest endorsement, approval , sponsorship, or association unless explicitly agreed to by Springer Nature in writing;
4. use bots or other automated methods to access the content or redirect messages
5. override any security feature or exclusionary protocol; or
6. share the content in order to create substitute for Springer Nature products or services or a systematic database of Springer Nature journal content.

In line with the restriction against commercial use, Springer Nature does not permit the creation of a product or service that creates revenue, royalties, rent or income from our content or its inclusion as part of a paid for service or for other commercial gain. Springer Nature journal content cannot be used for inter-library loans and librarians may not upload Springer Nature journal content on a large scale into their, or any other, institutional repository.

These terms of use are reviewed regularly and may be amended at any time. Springer Nature is not obligated to publish any information or content on this website and may remove it or features or functionality at our sole discretion, at any time with or without notice. Springer Nature may revoke this licence to you at any time and remove access to any copies of the Springer Nature journal content which have been saved.

To the fullest extent permitted by law, Springer Nature makes no warranties, representations or guarantees to Users, either express or implied with respect to the Springer nature journal content and all parties disclaim and waive any implied warranties or warranties imposed by law, including merchantability or fitness for any particular purpose.

Please note that these rights do not automatically extend to content, data or other material published by Springer Nature that may be licensed from third parties.

If you would like to use or distribute our Springer Nature journal content to a wider audience or on a regular basis or in any other manner not expressly permitted by these Terms, please contact Springer Nature at

onlineservice@springernature.com